PMIP4 experiments using MIROC-ES2L Earth System Model

Rumi Ohgaito[1], Akitomo Yamamoto[1], Tomohiro Hajima[1], Ryouta O'ishi[2], Manabu Abe[1], Hiroaki Tatebe[1], Ayako Abe-Ouchi[2,3,1], Michio Kawamiya[1]

[1]Research Center for Environmental Modeling and Application, Japan Agency for Marine-Earth Science and Technology, 3173-25 Showamachi, Kanazawaku, Yokohama 236-0001, Japan
[2] Atmosphere and Ocean Research Institute, University of Tokyo, Kashiwa, 2778568, Japan
[3] National Institute of Polar Research, Tachikawa, 1908518, Japan

Correspondence to: Rumi Ohgaito (ohgaito@jamstec.go.jp)

Abstract. Following the protocol of the fourth phase of the Paleoclimate Modeling Intercomparison Project (PMIP4), we performed numerical experiments targeting distinctive past time periods using the Model for Interdisciplinary Research on Climate Earth System Model (MIROC-ES2L), which is an Earth System Model. Setup and basic performance of the experiments are presented.

The Last Glacial Maximum was one of the most extreme climate states during the Quaternary and conducting numerical modeling experiments of this period has long been a challenge for the paleoclimate community. We conducted a Last Glacial Maximum experiment with a long spin-up of nearly 9,000 years. Globally, there is reasonable agreement between the anomalies relative to present day derived from model climatology and those derived from proxy data archives while some regional discrepancies remain.

By changing orbital and greenhouse gas forcings, we conducted experiments for two interglacial periods: 6,000 and 127,000 years before present. Model anomalies relative to present day are qualitatively consistent with variations in solar forcing. However, anomalies in the model are smaller than those derived from proxy data archives, suggesting that processes that play a role in past interglacial climates are still missing in this state-of-the-art model.

We conducted transient simulations from 850 CE to 1850 CE and from 1850 CE to 2014 CE. Cooling in the model indicates clear responses to huge volcanic eruptions, which are consistent with paleo-proxy data. The contrast between cooling during the Little Ice Age and warming during the 20th to 21st centuries is well represented at the multi-decadal time scale.

1 Introduction

Using climate models to model past climate provides unique opportunities to evaluate models' projections of future climate. The Paleoclimate Modeling Intercomparison Project (PMIP) began in the early 1990s (Joussaume et al., 1999). Since then, the paleoclimate community has continued to expand their research to include more time periods and events. With the increase of computational power, models of higher complexity are used to make future projections (Kawamiya et al., 2020).

Phase 3 of PMIP was endorsed by phase 5 of the Coupled Model Intercomparison Project (CMIP5; Braconnot et al., 2012),
and PMIP is now in its fourth phase (PMIP4; Kageyama et al., 2018). The proposed PMIP4 experiments cover a wide range

35 of time periods, including the Last Glacial Maximum (LGM; 21,000 years before present), two interglacials (6,000 and
127,000 years before present), the last millennium (LM), the Pliocene and many non-CMIP time periods.

The Quaternary is characterized by cyclic climate change with long glacials and short interglacials that have been recorded
in various paleo-proxy records, such as ice cores (Jouzel et al., 2007; Dome Fuji Ice Core Project Members, 2017), ocean
sediment cores (Weldeab et al., 2007), loess records (Maher et al., 2010), and terrestrial fossils (Bartlein et al., 2011). The

40 LGM refers to the period when global ice volume reached its maximum. It was also one of the coldest periods of the
Quaternary.

Since the beginning of PMIP, attention has been drawn towards the LGM, which was one of the extreme periods in the
glacial–interglacial cycles of the Quaternary (Joussaume and Taylor, 2000; Braconnot et al., 2007; Kageyama et al., 2020)
and also the most recent period during which global coverage of the continental ice sheets was at its maximum and

45 greenhouse gas (GHG) levels were at the minimum.

Because cooling at LGM relative to PI is at a comparable level to present-day global warming, LGM modeling can provide
useful information to constrain climate sensitivity for projections of future climate (Annan et al., 2006; Martin et al., 2020).
Intercomparison studies of proxy-based reconstructions of climate variables and model output continue to be conducted
(Braconnot et al., 2007; Bartlein et al., 2011; Kageyama et al., 2020). They report good agreement between model output and

50 proxy data for temperature and SST anomalies over the low latitudes (Otto-Bliesner et al., 2009; Hargreaves et al., 2013); the
tendency for models to underestimate cooling over Greenland (Masson-Delmotte et al., 2006) remains. Models have
difficulty to reproduce the weakened Atlantic meridional overturning circulation (AMOC) at LGM (Weber, 2007; Brady et
al. 2013; Muglia and Schmittner, 2015; Marzocchi and Jansen, 2017) and/or dust emission (Mahowald et al., 2006; Hopcroft
et al., 2015; Albani et al., 2014; Ohgaito et al., 2018), which may influence their simulations of temperature anomaly.

55 The interglacial periods of 6,000 and 127,000 years before present are characterized by differences in solar radiation at the
top of the atmosphere caused by orbital states that were different from those of the present day (Brierley et al., 2020; Otto-
Bliesner et al., 2020), resulting in seasonalities that were different from the pre-industrial period (1850 CE). Because it was
in the recent past and various paleo-proxy records are available (Ritchie et al., 1985; Drake et al., 2011; Hely et al., 2014;
Tierney et al. 2013, 2017), the interglacial period of 6,000 years before present was the only interglacial included in earlier

60 phases of PMIP (Braconnot et al., 2007; Ohgaito and Abe-Ouchi, 2007, 2009; Ohgaito et al., 2013). As a result of efforts to
collect paleo-proxy data (Otto-Bliesner et al., 2001; Lunt et al., 2013; Capron et al., 2014, 2017), it is now also possible to
conduct the same experiment for 127,000 years before present; experiments of this interglacial period have the advantage of
strong seasonality in the Northern Hemisphere (NH). The insolation anomaly at 127,000 years before present is larger than
that at 6,000 years before present; the stronger summer insolation at 127,000 years before present during boreal summer

65 modulates temperature and circulation for that time period (Lunt et al., 2013). The role of vegetation coupling has been
discussed intensively as studies report that vegetation enhances warming in the NH (O'ishi and Abe-Ouchi, 2011) and

precipitation over the Sahara Desert (Braconnot et al., 2000; Hopcroft et al., 2017). However, models have been unable to reproduce the quantitative changes recorded in proxy data.

70   Because the LM is the most recent period prior to the pre-industrial, there are vast amounts and varieties of proxy records from exact times in proxy data (PAGES2k-PMIP3 group, 2015; Luterbacher et al., 2016; Gagan et al., 2016) and in the literature (Pfister and Brazdil, 2006; Xoplaki et al., 2016; Camenisch et al., 2016). In earlier numerical paleoclimate studies, simple models were used to conduct transient experiments over periods of 1,000 years (Crowley, 2000; Goosse et al., 2005). With the increase of computational power, simulations using coupled Atmosphere–Ocean General Circulation Models

75   (AOGCMs) and/or comprehensive earth system models (ESMs) became standard. Coordination of LM experiments began under PMIP3 (Schmidt et al., 2012) and multiple AOGCMs and ESMs have been used to perform LM experiments. One of the important questions for LM experiments is whether climate variabilities stem from internal variability or forced responses. Atwood et al. (2016) decomposed the forcing of the LM experiment and concluded that cooling during the Little Ice Age (LIA; 1450–1850 CE) was largely driven by volcanic eruptions. PAGES2k (2015) summarized reconstruction–

80   model intercomparisons and reported that the agreement between model and proxy-based reconstructions is better in the high latitudes in the Northern Hemisphere and worse in the Southern Hemisphere. Historical (HIST; 1850–2014 CE) and LM experiments are intrinsically different from the other PMIP4 time-slice experiments discussed in this paper. They are time varying experiments that follow the same method used in the historical experiment in CMIP6. Hence, the LM experiment is closely aligned with the scientific focus of other endorsed MIPs, such as comparison of climatic response to volcanic forcing

85   (VolMIP; Zanchettin et al., 2016) and land use (LUMIP; Lawrence et al., 2016).

    Using the Model for Interdisciplinary Research on Climate Earth System version 2 for Long-term simulations (MIROC-ES2L), we performed numerical experiments targeting distinctive time periods. These include the LGM, the 6ka and the 127ka experiments and the LM. The MIROC-ES2L is an ESM that contains atmosphere, ocean, land, and ocean and land biogeochemical cycles (Hajima et al. 2020) and has been developed recently to contribute to CMIP6 and the United Nations

90   Intergovernmental Panel on Climate Change Sixth Assessment Report.

    The model is presented in Sect. 2 and the experimental setup and spin-up procedures are explained in Sect. 3. Basic climate states from the experiments are presented in Sect. 4 and conclusions and outlook are discussed in Sect. 5.

2 Model

    The MIROC-ES2L is an ESM developed for CMIP6 (Hajima et al. 2020) and its physical core comprises an atmosphere, an

95   ocean and a land module; variables are exchanged via a flux coupler (Fig. 1). The AOGCM components are the same as those in Tatebe et al. (2018). The physical ocean and land modules are coupled with the land ecosystem model VISIT-e (Ito and Inatomi, 2012) and the ocean biogeochemical model OECO2 with a nutrient–phytoplankton–zooplankton–detritus type representation of the ecosystem. The ecosystem modules can simulate global carbon and nitrogen cycles explicitly.

Distribution of plant functional types (PFTs) is prescribed because VISIT-e is not a dynamic vegetation model. Dynamics of
aerosols are calculated by an online aerosol module, SPRINTARS (Takemura et al., 2000, 2004, 2009).

Horizontal resolution of the atmosphere is set to T42 spectral truncation. Vertical resolution is 40 levels up to 3 hPa. The
ocean component has tripolar horizontal coordinates, with two poles in the NH that are located over land to avoid singularity
over ocean grids. Horizontal resolution of the ocean is 1° longitude and varies from 0.5° latitude around the Equator to 1°
latitude over the midlatitudes. Vertical resolution of the ocean is 62 layers with a hybrid sigma-z coordinate.

Using this model, various types of CMIP6 experiments have been performed. These include all of the Diagnostic,
Evaluation and Characterization of Klima (DECK) experiments, the historical experiment and the endorsed MIP experiments.

3. Experimental setup and spin-up procedures

3.1 setup and spin-up of pre-industrial control experiment

The pre-industrial (PI) control experiment is the reference experiment of all the paleoclimate experiments. It is identical to
the piControl experiment in CMIP6 (Eyring et al., 2016) and the experimental configuration of PI in MIROC-ES2L is
described in detail in Hajima et al. (2019). Levels of GHGs were set following the protocol of CMIP6: CO_2, CH_4 and N_2O
were set to 284.725 ppm, 808.25 ppb and 273.02 ppb, respectively (Table 1). The experiment was run for more than 9,000
model years during the course of model development and the final drift of the global mean surface air temperature is
-4.79×10^{-5} °C yr^{-1} for the last 500 years (Hajima et al. 2020). Model output from this period was submitted to CMIP6 and
the climatology of this period is used for the analyses in this study.

3.2 setup and spin-up of Last Glacial Maximum experiment

We performed a LGM experiment following PMIP4 protocol (Kageyama et al., 2017). A long spin-up is essential because of
the considerable differences between LGM and present day conditions. Hence, before model development was finalized, we
started spinning up using the physical core (AOGCM) of MIROC-ES2L (Tatebe et al., 2018). Spin-up started with reducing
CO_2 (Bereiter et al., 2015), CH_4 (Loulergue et al., 2008) and N_2O (Schilt et al., 2010) levels from PI to LGM values (Table
1). Global mean air temperature gradually reached quasi-equilibrium. After integration for 2,640 model years, the land–sea
mask, ice sheets, altitude (from ICE-6G_C as presented in Peltier et al., 2015), river courses and Earth's orbit (Berger, 1978)
(Fig. 3) were changed from PI to LGM conditions step by step, and total spin-up time is 6,760 model years (Fig. 2). Because
the development of MIROC-ES2L was finalized during LGM spin-up, conditions in the 6760th model year of the spin-up
were used to initiate the LGM experiment in MIROC-ES2L. In this conversion procedure, the offline terrestrial module was
spun up for 40,000 model years until quasi-stability was reached and the end state was used in the LGM experiment in
MIROC-ES2L. This was followed by spinning up the main MIROC-ES2L experiment for a further 100 years. Ocean salinity
(1 Practical Salinity Unit was added globally) and an erodibility map (addressing dust emission under LGM conditions as

4

130   proposed by Albani et al., 2016) were introduced. The erodibility map specifies low latitudes as deserts and middle to high

latitudes as tundra (Fig. 4). Land and ocean ecosystem models were spun up offline for 40,000 and 3,000 model years,

respectively, on the basis of the physical conditions created by MIROC-ES2L. Land and ocean biogeochemical state at the

end of the offline spin-up were used to initialize the LGM experiment in MIROC-ES2L. The LGM experiment was run for a

further 1,800 years until it eventually reached quasi-equilibrium. Surface air temperature of the last 500 model years shows a

135   trend of 0.0002 °C yr^{-1}. Model output from the last 100 years was submitted to PMIP4-CMIP6.

3.3 setup and spin-up of the two interglacial experiments

The 6ka and 127ka experiments were spun up following the protocol outlined in Otto-Bliesner et al. (2017). For the 6ka

experiment, CO_2, CH_4 and N_2O were set to 264.4 ppm, 597 ppb and 262 ppb; orbital parameters of eccentricity, obliquity

140   and precession were set to 0.018682, 24.105° and 0.87°. For the 127ka experiment, CO_2, CH_4 and N_2O were set to 275 ppm,

255 ppb and 685 ppb; eccentricity, obliquity and precession were set to 0.039378, 24.04° and 275.41° (Table 1).

Starting from PI, the 6ka experiment was integrated for 1,500 model years and the 127ka experiment was integrated for

1,550 model years (Fig. 2 (b), (c)). After the long spin-up, the last 100 years of the simulations were selected as the formal

products to be submitted to CMIP6 and for analyses in this study. The 127ka experiment is identical to the LIG experiment

145   in O'ishi et al. (2020).

3.4 setup and spin-up of the Last Millennium and historical experiments

We performed a LM experiment following the protocol of Jungclaus et al. (2017). The experiment was forced with time

varying total solar irradiance (Shapiro et al., 2011; Vieira et al., 2011; Wu et al., 2017), orbit (Berger, 1978), GHGs

150   (Meinshousen et al., 2017), volcanic eruptions (Sigl, 2015; Tooney and Sigl, 2017), ozone and land use change (Hurtte et al.,

2016). Table 2 summarizes the forcings for the LM experiment. The experiment basically followed the same procedure as

that of the historical experiment in CMIP6 (Eyring et al., 2016). From PI, the model was run under the constant forcing from

850 CE for 200 model years. The end state of the spin-up was used to initialize the time varying LM experiment, which was

conducted from 850 to 1850 CE. We performed a HIST experiment following CMIP6 protocol (Eyring et al., 2016). The end

155   state of the LM experiment was used to initialize HIST, which was run until 2014 CE.

4. Comparison of mean climate states derived from model output and paleoclimate proxy data archives

4.1 PI mean climate

Hajima et al. (2019) analyzed basic model performance for the present and indicated that MIROC-ES2L is a state-of-the art

ESM that is able to reproduce mean climatology reasonably well. Global annual mean air temperature at 2 m height is

160   14.99 °C and peak value of annual mean AMOC is 15.3 Sv, which falls within the range of reasonable estimates (Frajka-Williams et al., 2019). Model sea surface temperature (SST) represented reasonable global distribution but has a positive bias over the Southern Ocean, which leads to underestimation of Antarctic sea ice extent.

4.2 LGM mean climate

165   Relative to PI, the last 100 years of the LGM has a global mean surface air temperature anomaly of −4.4 °C (Fig. 5) and a tropical air temperature anomaly of about −2 °C, which is consistent with values derived from paleo-proxy archives (MARGO project members, 2009; Bartlein et al., 2011). Borehole thermometry suggested a temperature anomaly at LGM relative to PI over Eastern Antarctica of −7 to −10 °C (Stenni et al., 2010; Uemura et al., 2012). Temperature anomaly in the model is about −6.0 °C suggesting that cooling in the model is weak. For central Greenland, borehole thermometry suggested a temperature anomaly of −21 to −25 °C (Cuffey et al., 1995; Johnsen et al., 1995; Dahl-Jensen et al., 1998),

170   whereas model temperature anomaly is −11.1 °C. The large discrepancy between ice core data and model output could partly be attributed to issues related to the modeling of the thermohaline state of the ocean (McManus et al., 2004; Curry and Oppo, 2005). It is well known that numerical models have difficulty in reproducing the sluggish thermohaline circulation at LGM (Otto-Bliesner et al., 2007; Muglia and Schmittner, 2015; Sherriff-Tadano et al., 2017) that is suggested in proxy data

175   (Lynch-Stieglitz et al., 2007; Hesse et al., 2011). In our experiment, peak value of the annual mean AMOC at LGM is 21.0 Sv (Fig. 6), which is higher than that at PI. To address this issue, we will continue the experiment to identify the components that contribute to global cooling and those that contribute to cooling over the polar regions.

Figure 7 (b) shows net precipitation anomaly relative to PI. Total precipitation is 1063 mm yr^{-1} for LGM and 1166 mm yr^{-1} for PI. Consistent with Bartlein et al. (2011), model precipitation has a general tendency to be lower at the LGM than at PI

180   because lower SSTs and colder climate at the LGM result in a weaker hydrological cycle. Large reductions in precipitation relative to PI are found in areas that were covered by ice sheets at LGM but were no longer ice covered by PI, i.e. areas covered by the Laurentide and Fennoscandian ice sheets. These large anomalies would be associated with the higher altitude of the ice surface relative to the ground surface when the ice sheets have disappeared. In the northern North Atlantic Ocean, large anomalies are associated with the southward expansion of sea ice during the LGM.

185   Figure 8 shows primary production anomaly of the oceanic ecosystem of the LGM relative to PI with paleo-proxy data (Kohfeld et al., 2013) superimposed on model output. Because proxy data provide qualitative information rather than quantitative assessments, comparisons between model output and proxy data can only be used to evaluate the accuracy of the general direction of model anomaly. Positive model anomalies over the low to middle latitudes are consistent with proxy data. Negative anomalies over the high latitudes can be understood as the result of sea ice expansion at LGM. Sea ice

190   expansion at LGM is underestimated in the model (Crosta et al., 1998) and could result in negative anomalies around Antarctica that have smaller absolute values than those indicated by proxy data (Fig. 8).

An excessively weak positive anomaly around 40–50° S at LGM can be the result of dust emission being too high over South America in the PI experiment (Fig. 9). Mean global terrestrial gross primary production from the LGM experiment is 65 % of that from the PI experiment and is consistent with the estimates of Prentice et al. (2011), which were made using a

195 dynamic global vegetation model.

4.3 Mean changes in interglacial experiments

Figures 10 and 11 show air temperature and precipitation anomalies of 6ka and 127ka relative to PI. Because of the marked changes in seasonality in these time periods, average anomalies were calculated for June to August (JJA) and December to

200 February (DJF). Air temperature anomalies are positive over continental interiors in the middle to high latitudes in JJA for both 6ka (Fig. 10 (a)) and 127ka (Fig. 11 (a)) as a result of changes in shortwave radiation forcing. Compared with 6ka, stronger shortwave forcing results in larger air temperature anomalies in 127ka (Fig. 3).

Precipitation anomalies suggest that, relative to PI, boreal summer monsoons were stronger (Figs. 10 (b) and 11 (b)) and austral summer monsoons were weaker during the interglacials (Figs. 10 (d) and 11 (d)). Precipitation anomaly over the

205 Sahel region suggests that the reduction of desert area during the interglacials relative to PI is smaller in the model than that suggested by proxy data (Petit-Maire, 1999; Castaneda, 2009; Tierney et al., 2017; Drake et al., 2011; Hely et al., 2014), which is a mismatch that has been persistent through many modeling efforts (Braconnot et al., 2001, 2007).

Variations of temperature and precipitation anomalies with season and latitude are shown in four Hovmöller diagrams (Fig. 12). Temperature anomaly basically responds to changes in solar radiation with a lag of approximately a month (Figs. 3 (b,

210 c), 12 (a) and (b)), which could be the consequence of the slow thermal response of the ocean surface. Precipitation anomalies of 6ka and 127ka relative to PI exhibit a northward shift and enhancement during boreal summer in the NH (Fig. 12 (c) and (d)) which is consistent with Figs. 10 (b), 11.

4.4 Last Millennium and historical transient variabilities

215 Figure 13 shows the time series of annual mean NH air temperature of LM and HIST. Sharp cooling events are clear responses to huge volcanic eruptions. The effect of solar forcing on annual mean temperature is unclear probably because signals are small compared to internal variability.

The LIA is relatively well expressed in the NH mean but the warming during the Medieval Climate Anomaly (MCA; 950–1250 CE) that is suggested by proxy data is underestimated by the model. Difference between NH mean temperature at the

220 LIA and that at the MCA is −0.1 °C, which is not statistically significant in the Student's t-test.

The HIST experiment was run for the period between 1850 and 2014 CE. Fig. 13 also shows MIROC-ES2L historical experiments output submitted to CMIP6 and data from HadCRUT4 (Morice et al., 2012). Centennial variabilities of the NH

mean temperature in HIST and in CMIP6 historical experiments are very similar. There is also good agreement between HadCRUT4 data and output from all of the historical experiments at the multi-decadal time scale.

225

5. Outlook and conclusions

Using MIROC-ES2L, an ESM that has been recently developed for CMIP6, we performed numerical experiments to examine paleoclimate during several time periods and one historical experiment that was initiated from the LM experiment.

Globally, there is good agreement between the climate states described by the model and those derived from proxy data
230 while some regional discrepancies remain. In this section, we summarize the results and explore the possible causes of the discrepancies.

From PI, LGM conditions were introduced step by step into MIROC-ES2L and the LGM spin-up experiment was run for about 9,000 model years. Temperature anomaly of LGM relative to PI over the tropics is negative and there is general quantitative agreement between the anomaly derived from the model and that from proxy data (Bartlein et al., 2011;
235 MARGO project members, 2009).It has been pointed out in the United Nations Intergovernmental Panel on Climate Change (2013) Fifth Assessment Report that the cooling over Greenland at LGM relative to PI is underestimated in models. This could be attributed to a strong AMOC in the models, which leads to an estimate of sea ice expansion over the northern Atlantic Ocean that is lower than that suggested by proxy data. Intrusion of Antarctic bottom water into the Atlantic basin is very weak in MIROC-ES2L even in the PI experiment (Tatebe et al., 2018). Insufficient abyssal flow into the Atlantic basin
240 could be partly caused by the low resolution of the ocean component. Positive SST bias over the Southern Ocean in the model at PI may also contribute towards the underestimation of abyssal flow and could result in a persistently strong AMOC at LGM. Detailed analyses on representation of atmospheric circulations would be necessary for further investigations. Model representation of the Southern Ocean may influence the distribution of CO_2 between atmosphere and ocean (Moore et al., 2000). Anomalies associated with topography may be obscured by the low horizontal resolution of the model resulting in
245 discrepancies between climate states in the model and those derived from proxy data. Cooling of Eastern Antarctica at LGM relative to PI that is suggested by ice core data is underestimated by the model. This could be partly attributed to the positive SST bias over the Southern Ocean in the model at PI and the subsequent underestimation of sea ice expansion.

There is reasonable agreement between dust flux from the LGM experiment and that suggested by proxy data. However, the PI experiment overestimates dust emissions from South America. Thus, the change in dust emission between LGM and
250 PI is likely to be underestimated in the model, leading to underestimates of LGM anomalies relative to PI for climate (Ohgaito et al., 2018) and ecosystem activity in the Southern Ocean (Yamamoto et al., 2019).

We prescribed conventional land PFTs in the LGM experiment. In models that comprise a coupled dynamic vegetation model, climate states would be altered by biophysical feedback as a result of changes in vegetation cover (O'ishi and Abe-Ouchi, 2013).

255   The LGM experiment was also performed in the previous phase of PMIP using MIROC-ESM (Sueyoshi et al., 2013), which is the previous version of MIROC-ES2L. Because of differences in forcing (mainly in GHGs and ice sheets) and spin-up procedures we are unable to make direct comparisons of the experiments conducted using the two versions of the model. However, there is a general tendency of the PMIP4 model to simulate less cooling at LGM relative to PI, which is a tendency that was also identified by Kageyama et al. (2020) in their comparison of LGM experiments from different versions of PMIP.

260   Further sensitivity experiments using different boundary conditions could be helpful for identifying causes of this discrepancy.

The two interglacial experiments – 6ka and 127ka – include different orbital parameters and GHG levels and have long spin-up times that exceed 1,500 years. Results show warming over NH continents during boreal summer relative to PI. This is consistent with the direction of change suggested by proxy archives (Bartlein et al., 2011; Turney and Jones, 2010) but the

265   model underestimates the amount of warming. The discrepancy may be reduced by improving experimental setups, such as replacing the prescription of PFTs by a process that can produce PFTs that are closer to the real conditions of the periods. Although this could be partially achieved by including a dynamic vegetation model into ESMs (O'ishi and Abe-Ouchi, 2011; O'ishi et al., 2020), the degree of improvement would be area dependent.

Compared with PI, temperature over the tropics is lower in the 6ka experiment, which contradicts with proxy data.

270   However, cooling over the tropics can be considered as a reasonable and direct response to net negative solar forcing. Thus, the discrepancy between the model and proxy data suggests that feedbacks that may play a role in modeling climate change are missing in the current model. Further improvement and expansion of the model would be necessary.

Precipitation anomaly shows a northward shift of peak precipitation in boreal summer in the NH. Precipitation anomaly over the Sahara Desert in the model is still smaller than that suggested by proxy data archive, which is a mismatch that has been

275   persistent throughout the long history of PMIP. It may be necessary to include new processes to maintain high soil moisture in the interglacials (Hopcroft et al., 2017).

The LM experiment performed in this study shows clear responses of global temperature to huge volcanic eruptions while responses of global temperature to other forcings are unclear. Responses to external forcings except volcanos are likely to be small compared with internal variabilities.

280   Difference between model NH mean temperature at the LIA and that at the MCA is too small to be statistically significant. However, earlier studies suggested that signals may be more pronounced at regional scales (PAGES2k, 2015; Fernandez-Donado et al., 2013). Further investigations in regional scales would be necessary. The HIST experiment was initiated from the end of the LM experiment and produces time series of global temperatures that are similar to those from the other historical experiments that were initiated from PI (Hajima et al. 2020). This suggests that the initial conditions used for the

285   standard historical experiment in CMIP6 are appropriate for the simulation of global temperatures in the industrial era. Sensitivity experiments using different boundary conditions will be useful for identifying causalities to obtain more details in future analyses.

Data availability

290   The source code of MIROC-ES2L can be obtained from https://zenodo.org/record/3893386#.XuW9icvnhaQ. The source codes of the analyses and required input data can be found at https://zenodo.org/record/3893403#.XuY5CcvnhaQ. The DOIs of the time slice experiments are listed in Table 1. DOI for LM and HIST experiments are 10.22033/ESGF/CMIP6.5666 and /10.22033/ESGF/CMIP6.5602. The model output performed in this study are freely available through the Earth System Grid Federation (ESGF). Details on the ESGF can be found on the website of the CMIP Panel (https://www.wcrp-

295 climate.org/wgcm-cmip/wgcm-cmip6, last access: 13 June 2020).

Author contribution

RuO coordinated, prepared the boundaries, conducted the LGM, 6ka and LM, analyzed the experiments and wrote the manuscript. AY conducted offline spin-up of the ocean ecosystem experiments for LGM and analyzed the outputs. TH developed and provided MIROC-ES2L and the offline land ecosystem model and advised for

300 conducting experiments. RyO conducted the 127ka experiment. MA prepared most of the boundary conditions of LM experiment and submitted the data for ESGF. HT helped to prepare the ocean mask for LGM experiment. All authors contributed to discussions and to improve the manuscript.

Competing interests

305 The authors declare no competing interests.

References

Albani, S., Mahowald, N. M., Perry, A. T., Scanza, R. A., Zender, C. S., Heavens, N. G., Maggi, V., Kok, J. F., and Otto-Bliesner, B. L.: Improved dust representation in the Community Atmosphere Model, Journal of Advances in Modeling Earth Systems, 6, 541-570, doi:10.1002/2013ms000279, 2014.

Albani, S., Mahowald, N. M., Murphy, L. N., Raiswell, R., Moore, J. K., Anderson, R. F., McGee, D., Bradtmiller, L. I., Delmonte, B., Hesse, P. P., and Mayewski, P. A.: Paleodust variability since the Last Glacial Maximum and implications for iron inputs to the ocean, Geophysical Research Letters, 43, 3944-3954, doi:10.1002/2016gl067911, 2016.

Annan, J. D., and Hargreaves, J. C.: Using multiple observationally-based constraints to estimate climate sensitivity, Geophysical Research Letters, 33, doi:10.1029/2005gl025259, 2006.

Atwood, A. R., Wu, E., Frierson, D. M. W., Battisti, D. S., and Sachs, J. P.: Quantifying Climate Forcings and Feedbacks over the Last Millennium in the CMIP5-PMIP3 Models, Journal of Climate, 29, 1161-1178, doi:10.1175/jcli-d-15-0063.1, 2016.

Bartlein, P. J., Harrison, S. P., Brewer, S., Connor, S., Davis, B. A. S., Gajewski, K., Guiot, J., Harrison-Prentice, T. I., Henderson, A., Peyron, O., Prentice, I. C., Scholze, M., Seppa, H., Shuman, B., Sugita, S., Thompson, R. S., Viau, A. E., Williams, J., and Wu, H.: Pollen-based continental climate reconstructions at 6 and 21 ka: a global synthesis, Climate Dynamics, 37, 775-802, doi:10.1007/s00382-010-0904-1, 2011.

Bereiter, B., Eggleston, S., Schmitt, J., Nehrbass-Ahles, C., Stocker, T. F., Fischer, H., Kipfstuhl, S., and Chappellaz, J.: Revision of the EPICA Dome C CO2 record from 800 to 600kyr before present, Geophysical Research Letters, 42, 542-549, doi:10.1002/2014gl061957, 2015.

Berger, A. L.: LONG-TERM VARIATIONS OF DAILY INSOLATION AND QUATERNARY CLIMATIC CHANGES, Journal of the Atmospheric Sciences, 35, 2362-2367, doi:10.1175/1520-0469(1978)035<2362:ltvodi>2.0.co;2, 1978.

Bothe, O., Evans, M., Donado, L. F., Bustamante, E. G., Gergis, J., Gonzalez-Rouco, J. F., Goosse, H., Hegerl, G., Hind, A., Jungclaus, J., Kaufman, D., Lehner, F., McKay, N., Moberg, A., Raible, C. C., Schurer, A., Shi, F., Smerdon, J. E., von Gunten, L., Wagner, S., Warren, E., Widmann, M., Yiou, P., Zorita, E., and Grp, P. k.-P.: Continental-scale temperature variability in PMIP3 simulations and PAGES 2k regional temperature reconstructions over the past millennium, Climate of the Past, 11, 1673-1699, doi:10.5194/cp-11-1673-2015, 2015.

Braconnot, P., Joussaume, S., de Noblet, N., and Ramstein, G.: Mid-holocene and Last Glacial Maximum African monsoon changes as simulated within the Paleoclimate Modelling Intercomparison Project, Global and Planetary Change, 26, 51-66, 2000.

Braconnot, P., Otto-Bliesner, B., Harrison, S., Joussaume, S., Peterchmitt, J. Y., Abe-Ouchi, A., Crucifix, M., Driesschaert, E., Fichefet, T., Hewitt, C. D., Kageyama, M., Kitoh, A., Laine, A., Loutre, M. F., Marti, O., Merkel, U., Ramstein, G., Valdes, P., Weber, S. L., Yu, Y., and Zhao, Y.: Results of PMIP2 coupled simulations of the Mid-Holocene and Last Glacial Maximum - Part 1: experiments and large-scale features, Climate of the Past, 3, 261-277, 2007.

Braconnot, P., Harrison, S. P., Kageyama, M., Bartlein, P. J., Masson-Delmotte, V., Abe-Ouchi, A., Otto-Bliesner, B., and Zhao, Y.: Evaluation of climate models using palaeoclimatic data, Nature Climate Change, 2, 417-424, doi:10.1038/nclimate1456, 2012.

Brady, E. C., Otto-Bliesner, B. L., Kay, J. E., and Rosenbloom, N.: Sensitivity to Glacial Forcing in the CCSM4, Journal of Climate, 26, 1901-1925, doi:10.1175/jcli-d-11-00416.1, 2013.

Brierley, C. M., Zhao, A., Harrison, S. P., Braconnot, P., Williams, C. J. R., Thornalley, D. J. R., Shi, X., Peterschmitt, J.-Y., Ohgaito, R., Kaufman, D. S., Kageyama, M., Hargreaves, J. C., Erb, M. P., Emile-Geay, J., D'Agostino, R., Chandan, D., Carré, M., Bartlein, P., Zheng, W., Zhang, Z., Zhang, Q., Yang, H., Volodin, E. M., Tomas, R. A., Routson, C., Peltier, W. R., Otto-Bliesner, B., Morozova, P. A., McKay, N. P., Lohmann, G., Legrande, A. N., Guo, C., Cao, J., Brady, E., Annan, J. D., and Abe-Ouchi, A.: Large-scale features and evaluation of the PMIP4-CMIP6 *midHolocene* simulations, Clim. Past Discuss., https://doi.org/10.5194/cp-2019-168, in review, 2020.

Camenisch, C., Keller, K. M., Salvisberg, M., Amann, B., Bauch, M., Blumer, S., Brazdil, R., Bronnimann, S., Buntgen, U., Campbell, B. M. S., Fernandez-Donado, L., Fleitmann, D., Glaser, R., Gonzalez-Rouco, F., Grosjean, M., Hoffmann, R. C., Huhtamaa, H., Joos, F., Kiss, A., Kotyza, O., Lehner, F., Luterbacher, J., Maughan, N., Neukom, R., Novy, T., Pribyl, K., Raible, C. C., Riemann, D., Schuh, M., Slavin, P., Werner, J. P., and Wetter, O.: The 1430s: a cold period of extraordinary internal climate variability during the early Sporer Minimum with social and economic impacts in north-western and central Europe, Climate of the Past, 12, 2107-2126, doi:10.5194/cp-12-2107-2016, 2016.

Capron, E., Govin, A., Stone, E. J., Masson-Delmotte, V., Mulitza, S., Otto-Bliesner, B., Rasmussen, T. L., Sime, L. C., Waelbroeck, C., and Wolff, E. W.: Temporal and spatial structure of multi-millennial temperature changes at high latitudes during the Last Interglacial, Quaternary Science Reviews, 103, 116-133, doi:10.1016/j.quascirev.2014.08.018, 2014.

Capron, E., Govin, A., Feng, R., Otto-Bliesner, B. L., and Wolff, E. W.: Critical evaluation of climate syntheses to benchmark CMIP6/PMIP4 127 ka Last Interglacial simulations in the high-latitude regions, Quaternary Science Reviews, 168, 137-150, doi:10.1016/j.quascirev.2017.04.019, 2017.

Castaneda, I. S., Mulitza, S., Schefuss, E., dos Santos, R. A. L., Damste, J. S. S., and Schouten, S.: Wet phases in the Sahara/Sahel region and human migration patterns in North Africa, Proceedings of the National Academy of Sciences of the United States of America, 106, 20159-20163, doi:10.1073/pnas.0905771106, 2009.

Crosta, X., Pichon, J. J., and Burckle, L. H.: Application of modern analog technique to marine Antarctic diatoms: Reconstruction of maximum sea-ice extent at the Last Glacial Maximum, Paleoceanography, 13, 284-297, doi:10.1029/98pa00339, 1998.

Crowley, T. J.: Causes of climate change over the past 1000 years, Science, 289, 270-277, doi:10.1126/science.289.5477.270, 2000.

Cuffey, K. M., Clow, G. D., Alley, R. B., Stuiver, M., Waddington, E. D., and Saltus, R. W.: LARGE ARCTIC TEMPERATURE-CHANGE AT THE WISCONSIN-HOLOCENE GLACIAL TRANSITION, Science, 270, 455-458, 1995.

Curry, W. B., and Oppo, D. W.: Glacial water mass geometry and the distribution of delta C-13 of Sigma CO2 in the western Atlantic Ocean, Paleoceanography, 20, doi:10.1029/2004pa001021, 2005.

DahlJensen, D., Mosegaard, K., Gundestrup, N., Clow, G. D., Johnsen, S. J., Hansen, A. W., and Balling, N.: Past temperatures directly from the Greenland Ice Sheet, Science, 282, 268-271, 1998.

Drake, N. A., Blench, R. M., Armitage, S. J., Bristow, C. S., and White, K. H.: Ancient watercourses and biogeography of the Sahara explain the peopling of the desert, Proceedings of the National Academy of Sciences of the United States of America, 108, 458-462, doi:10.1073/pnas.1012231108, 2011.

390   Eyring, V., Gleckler, P. J., Heinze, C., Stouffer, R. J., Taylor, K. E., Balaji, V., Guilyardi, E., Joussaume, S., Kindermann, S., Lawrence, B. N., Meehl, G. A., Righi, M., and Williams, D. N.: Towards improved and more routine Earth system model evaluation in CMIP, Earth System Dynamics, 7, 813-830, doi:10.5194/esd-7-813-2016, 2016.

Frajka-Williams, E., Ansorge, I. J., Baehr, J., Bryden, H. L., Chidichimo, M. P., Cunningham, S. A., Danabasoglu, G., Dong, S. F., Donohue, K. A., Elipot, S., Heimbach, P., Holliday, N. P., Hummels, R., Jackson, L. C., Karstensen, J., Lankhorst, M., Le Bras, I. A., Lozier, M. S., McDonagh, E. L., Meinen, C. S., Mercier, H., Moat, B. I., Perez, R. C., 395   Piecuch, C. G., Rhein, M., Srokosz, M. A., Trenberth, K. E., Bacon, S., Forget, G., Goni, G., Kieke, D., Koelling, J., Lamont, T., McCarthy, G. D., Mertens, C., Send, U., Smeed, D. A., Speich, S., van den Berg, M., Volkov, D., and Wilson, C.: Atlantic Meridional Overturning Circulation: Observed Transport and Variability, Frontiers in Marine Science, 6, doi:10.3389/fmars.2019.00260, 2019.

Gagen, M. H., Zorita, E., McCarroll, D., Zahn, M., Young, G. H. F., and Robertson, I.: North Atlantic summer storm 400   tracks over Europe dominated by internal variability over the past millennium, Nature Geoscience, 9, 630-+, doi:10.1038/ngeo2752, 2016.

Goosse, H., Renssen, H., Timmermann, A., and Bradley, R. S.: Internal and forced climate variability during the last millennium: a model-data comparison using ensemble simulations, Quaternary Science Reviews, 24, 1345-1360, doi:10.1016/j.quascirev.2004.12.009, 2005.

405   Hajima, T., Watanabe, M., Yamamoto, A., Tatebe, H., Noguchi, M. A., Abe, M., Ohgaito, R., Ito, A., Yamazaki, D., Okajima, H., Ito, A., Takata, K., Ogochi, K., Watanabe, S., and Kawamiya, M.: Description of the MIROC-ES2L Earth system model and evaluation of its climate–biogeochemical processes and feedbacks, Geosci. Model Dev., 13, 2197–2244, https://doi.org/10.5194/gmd-13-2197-2020, 2020.

Hargreaves, J. C., Annan, J. D., Ohgaito, R., Paul, A., and Abe-Ouchi, A.: Skill and reliability of climate model ensembles 410   at the Last Glacial Maximum and mid-Holocene, Climate of the Past, 9, 811-823, doi:10.5194/cp-9-811-2013, 2013.

Hely, C., Lezine, A. M., and Contributors, A. P. D.: Holocene changes in African vegetation: tradeoff between climate and water availability, Climate of the Past, 10, 681-686, doi:10.5194/cp-10-681-2014, 2014.

Hesse, T., Butzin, M., Bickert, T., and Lohmann, G.: A model-data comparison of delta C-13 in the glacial Atlantic Ocean, Paleoceanography, 26, doi:10.1029/2010pa002085, 2011.

415   Hopcroft, P. O., and Valdes, P. J.: Last glacial maximum constraints on the Earth System model HadGEM2-ES, Climate Dynamics, 45, 1657-1672, doi:10.1007/s00382-014-2421-0, 2015.

Hopcroft, P. O., Valdes, P. J., Harper, A. B., and Beerling, D. J.: Multi vegetation model evaluation of the Green Sahara climate regime, Geophysical Research Letters, 44, 6804-6813, doi:10.1002/2017gl073740, 2017.

Hurtt, G. C., Thomas, R. Q., Fisk, J. P., Dubayah, R. O., and Sheldon, S. L.: The Impact of Fine-Scale Disturbances on the 420   Predictability of Vegetation Dynamics and Carbon Flux, Plos One, 11, doi:10.1371/journal.pone.0152883, 2016.

Ito, A., and Inatomi, M.: Use of a process-based model for assessing the methane budgets of global terrestrial ecosystems and evaluation of uncertainty, Biogeosciences, 9, 759-773, doi:10.5194/bg-9-759-2012, 2012.

Johnsen, S. J., Dahljensen, D., Dansgaard, W., and Gundestrup, N.: GREENLAND PALEOTEMPERATURES DERIVED FROM GRIP BORE HOLE TEMPERATURE AND ICE CORE ISOTOPE PROFILES, Tellus Series B-Chemical and
425 Physical Meteorology, 47, 624-629, doi:10.1034/j.1600-0889.47.issue5.9.x, 1995.

Joussaume, S., Taylor, K. E., Braconnot, P., Mitchell, J. F. B., Kutzbach, J. E., Harrison, S. P., Prentice, I. C., Broccoli, A. J., Abe-Ouchi, A., Bartlein, P. J., Bonfils, C., Dong, B., Guiot, J., Herterich, K., Hewitt, C. D., Jolly, D., Kim, J. W., Kislov, A., Kitoh, A., Loutre, M. F., Masson, V., McAvaney, B., McFarlane, N., de Noblet, N., Peltier, W. R., Peterschmitt, J. Y., Pollard, D., Rind, D., Royer, J. F., Schlesinger, M. E., Syktus, J., Thompson, S., Valdes, P., Vettoretti, G., Webb, R.
430 S., and Wyputta, U.: Monsoon changes for 6000 years ago: Results of 18 simulations from the Paleoclimate Modeling Intercomparison Project (PMIP), Geophysical Research Letters, 26, 859-862, doi:10.1029/1999gl900126, 1999.

Jouzel, J., Masson-Delmotte, V., Cattani, O., Dreyfus, G., Falourd, S., Hoffmann, G., Minster, B., Nouet, J., Barnola, J. M., Chappellaz, J., Fischer, H., Gallet, J. C., Johnsen, S., Leuenberger, M., Loulergue, L., Luethi, D., Oerter, H., Parrenin, F., Raisbeck, G., Raynaud, D., Schilt, A., Schwander, J., Selmo, E., Souchez, R., Spahni, R., Stauffer, B., Steffensen, J. P.,
435 Stenni, B., Stocker, T. F., Tison, J. L., Werner, M., and Wolff, E. W.: Orbital and millennial Antarctic climate variability over the past 800,000 years, Science, 317, 793-796, doi:10.1126/science.1141038, 2007.

Jungclaus, J. H., Bard, E., Baroni, M., Braconnot, P., Cao, J., Chini, L. P., Egorova, T., Evans, M., Gonzalez-Rouco, J. F., Goosse, H., Hurtt, G. C., Joos, F., Kaplan, J. O., Khodri, M., Goldewijk, K. K., Krivova, N., LeGrande, A. N., Lorenz, S. J., Luterbacher, J., Man, W. M., Maycock, A. C., Meinshausen, M., Moberg, A., Muscheler, R., Nehrbass-Ahles, C., Otto-
440 Bliesner, B. I., Phipps, S. J., Pongratz, J., Rozanov, E., Schmidt, G. A., Schmidt, H., Schmutz, W., Schurer, A., Shapiro, A. I., Sigl, M., Smerdon, J. E., Solanki, S. K., Timmreck, C., Toohey, M., Usoskin, I. G., Wagner, S., Wu, C. J., Yeo, K. L., Zanchettin, D., Zhang, Q., and Zorita, E.: The PMIP4 contribution to CMIP6-Part 3: The last millennium, scientific objective, and experimental design for the PMIP4 past1000 simulations, Geoscientific Model Development, 10, 4005-4033, doi:10.5194/gmd-10-4005-2017, 2017.

445 Kageyama, M., Albani, S., Braconnot, P., Harrison, S. P., Hopcroft, P. O., Ivanovic, R. F., Lambert, F., Marti, O., Peltier, W. R., Peterschmitt, J. Y., Roche, D. M., Tarasov, L., Zhang, X., Brady, E. C., Haywood, A. M., LeGrande, A. N., Lunt, D. J., Mahowald, N. M., Mikolajewicz, U., Nisancioglu, K. H., Otto-Bliesner, B. L., Renssen, H., Tomas, R. A., Zhang, Q., Abe-Ouchi, A., Bartlein, P. J., Cao, J., Li, Q., Lohmann, G., Ohgaito, R., Shi, X. X., Volodin, E., Yoshida, K., and Zheng, W. P.: The PMIP4 contribution to CMIP6-Part 4: Scientific objectives and experimental design of the PMIP4-CMIP6 Last
450 Glacial Maximum experiments and PMIP4 sensitivity experiments, Geoscientific Model Development, 10, 4035-4055, doi:10.5194/gmd-10-4035-2017, 2017.

Kageyama, M., Braconnot, P., Harrison, S. P., Haywood, A. M., Jungclaus, J. H., Otto-Bliesner, B. L., Peterschmitt, J. Y., Abe-Ouchi, A., Albani, S., Bartlein, P. J., Brierley, C., Crucifix, M., Dolan, A., Fernandez-Donado, L., Fischer, H., Hopcroft, P. O., Ivanovic, R. F., Lambert, F., Lunt, D. J., Mahowald, N. M., Peltier, W. R., Phipps, S. J., Roche, D. M.,
455 Schmidt, G. A., Tarasov, L., Valdes, P. J., Zhang, Q., and Zhou, T. J.: The PMIP4 contribution to CMIP6-Part 1: Overview and over-arching analysis plan, Geoscientific Model Development, 11, 1033-1057, doi:10.5194/gmd-11-1033-2018, 2018.

Kageyama, M., Harrison, S. P., Kapsch, M.-L., Löfverström, M., Lora, J. M., Mikolajewicz, U., Sherriff-Tadano, S., Vadsaria, T., Abe-Ouchi, A., Bouttes, N., Chandan, D., LeGrande, A. N., Lhardy, F., Lohmann, G., Morozova, P. A.,
460 Ohgaito, R., Peltier, W. R., Quiquet, A., Roche, D. M., Shi, X., Schmittner, A., Tierney, J. E., and Volodin, E.: The

PMIP4-CMIP6 Last Glacial Maximum experiments: preliminary results and comparison with the PMIP3-CMIP5 simulations, Clim. Past Discuss., https://doi.org/10.5194/cp-2019-169, in review, 2020.

Kawamura, K., Abe-Ouchi, A., Motoyama, H., Ageta, Y., Aoki, S., Azuma, N., Fujii, Y., Fujita, K., Fujita, S., Fukui, K., Furukawa, T., Furusaki, A., Goto-Azuma, K., Greve, R., Hirabayashi, M., Hondoh, T., Hori, A., Horikawa, S., Horiuchi,
465 K., Igarashi, M., Iizuka, Y., Kameda, T., Kanda, H., Kohno, M., Kuramoto, T., Matsushi, Y., Miyahara, M., Miyake, T., Miyamoto, A., Nagashima, Y., Nakayama, Y., Nakazawa, T., Nakazawa, F., Nishio, F., Obinata, I., Ohgaito, R., Oka, A., Okuno, J., Okuyama, J., Oyabu, I., Parrenin, F., Pattyn, F., Saito, F., Saito, T., Sakurai, T., Sasa, K., Seddik, H., Shibata, Y., Shinbori, K., Suzuki, K., Suzuki, T., Takahashi, A., Takahashi, K., Takahashi, S., Takata, M., Tanaka, Y., Uemura, R., Watanabe, G., Watanabe, O., Yamasaki, T., Yokoyama, K., Yoshimori, M., Yoshimoto, T., and Dome Fuji Ice Core, P.:
470 State dependence of climatic instability over the past 720,000 years from Antarctic ice cores and climate modeling, Science Advances, 3, doi:10.1126/sciadv.1600446, 2017.

Kohfeld, K. E., Graham, R. M., de Boer, A. M., Sime, L. C., Wolff, E. W., Le Quere, C., and Bopp, L.: Southern Hemisphere westerly wind changes during the Last Glacial Maximum: paleo-data synthesis, Quaternary Science Reviews, 68, 76-95, doi:10.1016/j.quascirev.2013.01.017, 2013.

475 Lawrence, D. M., Hurtt, G. C., Arneth, A., Brovkin, V., Calvin, K. V., Jones, A. D., Jones, C. D., Lawrence, P. J., de Noblet-Ducoudre, N., Pongratz, J., Seneviratne, S. I., and Shevliakova, E.: The Land Use Model Intercomparison Project (LUMIP) contribution to CMIP6: rationale and experimental design, Geoscientific Model Development, 9, 2973-2998, doi:10.5194/gmd-9-2973-2016, 2016.

Loulergue, L., Schilt, A., Spahni, R., Masson-Delmotte, V., Blunier, T., Lemieux, B., Barnola, J. M., Raynaud, D., Stocker,
480 T. F., and Chappellaz, J.: Orbital and millennial-scale features of atmospheric CH4 over the past 800,000 years, Nature, 453, 383-386, doi:10.1038/nature06950, 2008.

Lunt, D. J., Abe-Ouchi, A., Bakker, P., Berger, A., Braconnot, P., Charbit, S., Fischer, N., Herold, N., Jungclaus, J. H., Khon, V. C., Krebs-Kanzow, U., Langebroek, P. M., Lohmann, G., Nisancioglu, K. H., Otto-Bliesner, B. L., Park, W., Pfeiffer, M., Phipps, S. J., Prange, M., Rachmayani, R., Renssen, H., Rosenbloom, N., Schneider, B., Stone, E. J.,
485 Takahashi, K., Wei, W., Yin, Q., and Zhang, Z. S.: A multi-model assessment of last interglacial temperatures, Climate of the Past, 9, 699-717, doi:10.5194/cp-9-699-2013, 2013.

Luterbacher, J., Werner, J. P., Smerdon, J. E., Fernandez-Donado, L., Gonzalez-Rouco, F. J., Barriopedro, D., Ljungqvist, F. C., Buntgen, U., Zorita, E., Wagner, S., Esper, J., McCarroll, D., Toreti, A., Frank, D., Jungclaus, J. H., Barriendos, M., Bertolin, C., Bothe, O., Brazdil, R., Camuffo, D., Dobrovolny, P., Gagen, M., Garica-Bustamante, E., Ge, Q., Gomez-
490 Navarro, J. J., Guiot, J., Hao, Z., Hegerl, G. C., Holmgren, K., Klimenko, V. V., Martin-Chivelet, J., Pfister, C., Roberts, N., Schindler, A., Schurer, A., Solomina, O., von Gunten, L., Wahl, E., Wanner, H., Wetter, O., Xoplaki, E., Yuan, N., Zanchettin, D., Zhang, H., and Zerefos, C.: European summer temperatures since Roman times, Environmental Research Letters, 11, doi:10.1088/1748-9326/11/2/024001, 2016.

Lynch-Stieglitz, J., Adkins, J. F., Curry, W. B., Dokken, T., Hall, I. R., Herguera, J. C., Hirschi, J. J. M., Ivanova, E. V.,
495 Kissel, C., Marchal, O., Marchitto, T. M., McCave, I. N., McManus, J. F., Mulitza, S., Ninnemann, U., Peeters, F., Yu, E. F., and Zahn, R.: Atlantic meridional overturning circulation during the Last Glacial Maximum, Science, 316, 66-69, doi:10.1126/science.1137127, 2007.

Maher, B. A., Prospero, J. M., Mackie, D., Gaiero, D., Hesse, P. P., and Balkanski, Y.: Global connections between aeolian dust, climate and ocean biogeochemistry at the present day and at the last glacial maximum, Earth-Science Reviews, 99,
500 61-97, doi:10.1016/j.earscirev.2009.12.001, 2010.

15

Mahowald, N. M., Lamarque, J. F., Tie, X. X., and Wolff, E.: Sea-salt aerosol response to climate change: Last Glacial Maximum, preindustrial, and doubled carbon dioxide climates, Journal of Geophysical Research-Atmospheres, 111, doi:10.1029/2005jd006459, 2006.

505   Marzocchi, A., and Jansen, M. F.: Connecting Antarctic sea ice to deep-ocean circulation in modern and glacial climate simulations, Geophysical Research Letters, 44, 6286-6295, doi:10.1002/2017gl073936, 2017.

Marzocchi, A., and Jansen, M. F.: Global cooling linked to increased glacial carbon storage via changes in Antarctic sea ice, Nature Geoscience, 12, 1001-+, doi:10.1038/s41561-019-0466-8, 2019.

Masson-Delmotte, V., Kageyama, M., Braconnot, P., Charbit, S., Krinner, G., Ritz, C., Guilyardi, E., Jouzel, J., Abe-Ouchi, A., Crucifix, M., Gladstone, R. M., Hewitt, C. D., Kitoh, A., LeGrande, A. N., Marti, O., Merkel, U., Motoi, T., Ohgaito,
510   R., Otto-Bliesner, B., Peltier, W. R., Ross, I., Valdes, P. J., Vettoretti, G., Weber, S. L., Wolk, F., and Yu, Y.: Past and future polar amplification of climate change: climate model intercomparisons and ice-core constraints, Climate Dynamics, 26, 513-529, 2006.

McManus, J. F., Francois, R., Gherardi, J. M., Keigwin, L. D., and Brown-Leger, S.: Collapse and rapid resumption of Atlantic meridional circulation linked to deglacial climate changes, Nature, 428, 834-837, doi:10.1038/nature02494, 2004.

515   Meinshausen, M., Vogel, E., Nauels, A., Lorbacher, K., Meinshausen, N., Etheridge, D. M., Fraser, P. J., Montzka, S. A., Rayner, P. J., Trudinger, C. M., Krummel, P. B., Beyerle, U., Canadell, J. G., Daniel, J. S., Enting, I. G., Law, R. M., Lunder, C. R., O'Doherty, S., Prinn, R. G., Reimann, S., Rubino, M., Velders, G. J. M., Vollmer, M. K., Wang, R. H. J., and Weiss, R.: Historical greenhouse gas concentrations for climate modelling (CMIP6), Geoscientific Model Development, 10, 2057-2116, doi:10.5194/gmd-10-2057-2017, 2017.

520   Moore, J. K., Abbott, M. R., Richman, J. G., and Nelson, D. M.: The Southern Ocean at the last glacial maximum: A strong sink for atmospheric carbon dioxide, Global Biogeochemical Cycles, 14, 455-475, doi:10.1029/1999gb900051, 2000.

Morice, C. P., Kennedy, J. J., Rayner, N. A., and Jones, P. D.: Quantifying uncertainties in global and regional temperature change using an ensemble of observational estimates: The HadCRUT4 data set, Journal of Geophysical Research-
525   Atmospheres, 117, doi:10.1029/2011jd017187, 2012.

Muglia, J., and Schmittner, A.: Glacial Atlantic overturning increased by wind stress in climate models, Geophysical Research Letters, 42, 9862-9869, doi:10.1002/2015gl064583, 2015.

O'Ishi, R., and Abe-Ouchi, A.: Polar amplification in the mid-Holocene derived from dynamical vegetation change with a GCM, Geophysical Research Letters, 38, L14702, doi:10.1029/2011gl048001, 2011.

530   O'Ishi, R., and Abe-Ouchi, A.: Influence of dynamic vegetation on climate change and terrestrial carbon storage in the Last Glacial Maximum, Climate of the Past, 9, 1571-1587, doi:10.5194/cp-9-1571-2013, 2013.

O'ishi, R., Chan, W.-L., Abe-Ouchi, A., Sherriff-Tadano, S., and Ohgaito, R.: PMIP4/CMIP6 Last Interglacial simulations using different versions of MIROC, with and without vegetation feedback, Clim. Past Discuss., https://doi.org/10.5194/cp-2019-172, in review, 2020.
535   Ohgaito, R. and Abe-Ouchi, A.: The role of ocean thermodynamics and dynamics in Asian summer monsoon changes during the mid-Holocene, Clim. Dynam., 29, 39–50, 2007.

Ohgaito, R., and Abe-Ouchi, A.: The effect of sea surface temperature bias in the PMIP2 AOGCMs on mid-Holocene Asian monsoon enhancement, Climate Dynamics, 33, 975-983, doi:10.1007/s00382-009-0533-8, 2009.

540   Ohgaito, R., Sueyoshi, T., Abe-Ouchi, A., Hajima, T., Watanabe, S., Kim, H. J., Yamamoto, A., and Kawamiya, M.: Can an Earth System Model simulate better climate change at mid-Holocene than an AOGCM? A comparison study of MIROC-ESM and MIROC3, Climate of the Past, 9, 1519-1542, doi:10.5194/cp-9-1519-2013, 2013.

Ohgaito, R., Abe-Ouchi, A., O'Ishi, R., Takemura, T., Ito, A., Hajima, T., Watanabe, S., and Kawamiya, M.: Effect of high dust amount on surface temperature during the Last Glacial Maximum: a modelling study using MIROC-ESM, Climate of the Past, 14, 1565-1581, doi:10.5194/cp-14-1565-2018, 2018.

545   Otto-Bliesner, B. L., and Brady, E. C.: Tropical Pacific variability in the NCAR Climate System Model, Journal of Climate, 14, 3587-3607, doi:10.1175/1520-0442(2001)014<3587:tpvitn>2.0.co;2, 2001.

Otto-Bliesner, B. L., Schneider, R., Brady, E. C., Kucera, M., Abe-Ouchi, A., Bard, E., Braconnot, P., Crucifix, M., Hewitt, C. D., Kageyama, M., Marti, O., Paul, A., Rosell-Mele, A., Waelbroeck, C., Weber, S. L., Weinelt, M., and Yu, Y.: A comparison of PMIP2 model simulations and the MARGO proxy reconstruction for tropical sea surface temperatures at 550   last glacial maximum, Climate Dynamics, 32, 799-815, doi:10.1007/s00382-008-0509-0, 2009.

Otto-Bliesner, B. L., Braconnot, P., Harrison, S. P., Lunt, D. J., Abe-Ouchi, A., Albani, S., Bartlein, P. J., Capron, E., Carlson, A. E., Dutton, A., Fischer, H., Goelzer, H., Govin, A., Haywood, A., Joos, F., LeGrande, A. N., Lipscomb, W. H., Lohmann, G., Mahowald, N., Nehrbass-Ahles, C., Pausata, F. S. R., Peterschmitt, J. Y., Phipps, S. J., Renssen, H., and Zhang, Q.: The PMIP4 contribution to CMIP6-Part 2: Two interglacials, scientific objective and experimental design for 555   Holocene and Last Interglacial simulations, Geoscientific Model Development, 10, 3979-4003, doi:10.5194/gmd-10-3979-2017, 2017.

Peltier, W. R., Argus, D. F., and Drummond, R.: Space geodesy constrains ice age terminal deglaciation: The global ICE-6G_C (VM5a) model, Journal of Geophysical Research-Solid Earth, 120, 450-487, doi:10.1002/2014jb011176, 2015.

Petit-Maire, N.: Natural variability of the Earth's environments: the last two climatic extremes (18000 +/- 2000 and 8000 560   +/- 1000 yrs BP), Comptes Rendus De L Academie Des Sciences Serie Ii Fascicule a-Sciences De La Terre Et Des Planetes, 328, 273-+, doi:10.1016/s1251-8050(99)80307-3, 1999.

Pfister, C., and Brazdil, R.: Social vulnerability to climate in the "Little Ice Age": an example from Central Europe in the early 1770s, Climate of the Past, 2, 115-129, doi:10.5194/cp-2-115-2006, 2006.

Prentice, I. C., Harrison, S. P., and Bartlein, P. J.: Global vegetation and terrestrial carbon cycle changes after the last ice 565   age, New Phytologist, 189, 988-998, doi:10.1111/j.1469-8137.2010.03620.x, 2011.

Ritchie, J. C., Eyles, C. H., and Haynes, C. V.: SEDIMENT AND POLLEN EVIDENCE FOR AN EARLY TO MID-HOLOCENE HUMID PERIOD IN THE EASTERN SAHARA, Nature, 314, 352-355, doi:10.1038/314352a0, 1985.

Schilt, A., Baumgartner, M., Schwander, J., Buiron, D., Capron, E., Chappellaz, J., Loulergue, L., Schupbach, S., Spahni, R., Fischer, H., and Stocker, T. F.: Atmospheric nitrous oxide during the last 140,000 years, Earth and Planetary Science 570   Letters, 300, 33-43, doi:10.1016/j.epsl.2010.09.027, 2010.

17

Schmidt, G. A., Jungclaus, J. H., Ammann, C. M., Bard, E., Braconnot, P., Crowley, T. J., Delaygue, G., Joos, F., Krivova, N. A., Muscheler, R., Otto-Bliesner, B. L., Pongratz, J., Shindell, D. T., Solanki, S. K., Steinhilber, F., and Vieira, L. E. A.: Climate forcing reconstructions for use in PMIP simulations of the last millennium (v1.0), Geoscientific Model Development, 4, 33-45, doi:10.5194/gmd-4-33-2011, 2011.

575 Shapiro, A. I., Schmutz, W., Rozanov, E., Schoell, M., Haberreiter, M., Shapiro, A. V., and Nyeki, S.: A new approach to the long-term reconstruction of the solar irradiance leads to large historical solar forcing, Astronomy & Astrophysics, 529, doi:10.1051/0004-6361/201016173, 2011.

Sherriff-Tadano, S., Abe-Ouchi, A., Yoshimori, M., Oka, A., and Chan, W. L.: Influence of glacial ice sheets on the Atlantic meridional overturning circulation through surface wind change, Climate Dynamics, 50, 2881-2903, 580 doi:10.1007/s00382-017-3780-0, 2018.

Sigl, M., Winstrup, M., McConnell, J. R., Welten, K. C., Plunkett, G., Ludlow, F., Buentgen, U., Caffee, M., Chellman, N., Dahl-Jensen, D., Fischer, H., Kipfstuhl, S., Kostick, C., Maselli, O. J., Mekhaldi, F., Mulvaney, R., Muscheler, R., Pasteris, D. R., Pilcher, J. R., Salzer, M., Schuepbach, S., Steffensen, J. P., Vinther, B. M., and Woodruff, T. E.: Timing and climate forcing of volcanic eruptions for the past 2,500 years, Nature, 523, 543-+, doi:10.1038/nature14565, 2015.

585 Sueyoshi, T., Ohgaito, R., Yamamoto, A., Chikamoto, M. O., Hajima, T., Okajima, H., Yoshimori, M., Abe, M., O'Ishi, R., Saito, F., Watanabe, S., Kawamiya, M., and Abe-Ouchi, A.: Set-up of the PMIP3 paleoclimate experiments conducted using an Earth system model, MIROC-ESM, Geoscientific Model Development, 6, 819-836, doi:10.5194/gmd-6-819-2013, 2013.

Takemura, T., Okamoto, H., Maruyama, Y., Numaguti, A., Higurashi, A., and Nakajima, T.: Global three-dimensional 590 simulation of aerosol optical thickness distribution of various origins, Journal of Geophysical Research-Atmospheres, 105, 17853-17873, doi:10.1029/2000jd900265, 2000.

Takemura, T., Nozawa, T., Emori, S., Nakajima, T. Y., and Nakajima, T.: Simulation of climate response to aerosol direct and indirect effects with aerosol transport-radiation model, Journal of Geophysical Research-Atmospheres, 110, D02202, doi:10.1029/2004jd005029, 2005.

595 Takemura, T., Egashira, M., Matsuzawa, K., Ichijo, H., O'Ishi, R., and Abe-Ouchi, A.: A simulation of the global distribution and radiative forcing of soil dust aerosols at the Last Glacial Maximum, Atmospheric Chemistry and Physics, 9, 3061-3073, 2009.

Tatebe, H., Tanaka, Y., Komuro, Y., and Hasumi, H.: Impact of deep ocean mixing on the climatic mean state in the Southern Ocean, Scientific Reports, 8, doi:10.1038/s41598-018-32768-6, 2018.

600 Tierney, J. E., and deMenocal, P. B.: Abrupt Shifts in Horn of Africa Hydroclimate Since the Last Glacial Maximum, Science, 342, 843-846, doi:10.1126/science.1240411, 2013.

Tierney, J. E., Pausata, F. S. R., and deMenocal, P. B.: Rainfall regimes of the Green Sahara, Science Advances, 3, doi:10.1126/sciadv.1601503, 2017.

Uemura, R., Masson-Delmotte, V., Jouzel, J., Landais, A., Motoyama, H., and Stenni, B.: Ranges of moisture-source 605 temperature estimated from Antarctic ice cores stable isotope records over glacial-interglacial cycles, Climate of the Past, 8, 1109-1125, doi:10.5194/cp-8-1109-2012, 2012.

18

Vieira, L. E. A., Solanki, S. K., Krivova, N. A., and Usoskin, I.: Evolution of the solar irradiance during the Holocene, Astronomy & Astrophysics, 531, doi:10.1051/0004-6361/201015843, 2011.

610 Waelbroeck, C., Paul, A., Kucera, M., Rosell-Mele, A., Weinelt, M., Schneider, R., Mix, A. C., Abelmann, A., Armand, L., Bard, E., Barker, S., Barrows, T. T., Benway, H., Cacho, I., Chen, M. T., Cortijo, E., Crosta, X., de Vernal, A., Dokken, T., Duprat, J., Elderfield, H., Eynaud, F., Gersonde, R., Hayes, A., Henry, M., Hillaire-Marcel, C., Huang, C. C., Jansen, E., Juggins, S., Kallel, N., Kiefer, T., Kienast, M., Labeyrie, L., Leclaire, H., Londeix, L., Mangin, S., Matthiessen, J., Marret, F., Meland, M., Morey, A. E., Mulitza, S., Pflaumann, U., Pisias, N. G., Radi, T., Rochon, A., Rohling, E. J., Sbaffi, L., Schaefer-Neth, C., Solignac, S., Spero, H., Tachikawa, K., Turon, J. L., and Members, M. P.: Constraints on the magnitude
615 and patterns of ocean cooling at the Last Glacial Maximum, Nature Geoscience, 2, 127-132, doi:10.1038/ngeo411, 2009a.

Waelbroeck, C., Paul, A., Kucera, M., Rosell-Melee, A., Weinelt, M., Schneider, R., Mix, A. C., Abelmann, A., Armand, L., Bard, E., Barker, S., Barrows, T. T., Benway, H., Cacho, I., Chen, M. T., Cortijo, E., Crosta, X., de Vernal, A., Dokken, T., Duprat, J., Elderfield, H., Eynaud, F., Gersonde, R., Hayes, A., Henry, M., Hillaire-Marcel, C., Huang, C. C., Jansen, E., Juggins, S., Kallel, N., Kiefer, T., Kienast, M., Labeyrie, L., Leclaire, H., Londeix, L., Mangin, S., Matthiessen, J., Marret, F., Meland, M., Morey, A. E., Mulitza, S., Pflaumann, U., Pisias, N. G., Radi, T., Rochon, A., Rohling, E. J., Sbaffi, L.,
620 Schafer-Neth, C., Solignac, S., Spero, H., Tachikawa, K., Turon, J. L., and Members, M. P.: Constraints on the magnitude and patterns of ocean cooling at the Last Glacial Maximum, Nature Geoscience, 2, 127-132, doi:10.1038/ngeo411, 2009b.

Weber, S. L., Drijfhout, S. S., Abe-Ouchi, A., Crucifix, M., Eby, M., Ganopolski, A., Murakami, S., Otto-Bliesner, B., and Peltier, W. R.: The modern and glacial overturning circulation in the Atlantic Ocean in PMIP coupled model simulations,
625 Climate of the Past, 3, 51-64, 2007.

Weldeab, S., Schneider, R. R., and Muller, P.: Comparison of Mg/Ca- and alkenone-based sea surface temperature estimates in the fresh water-influenced Gulf of Guinea, eastern equatorial Atlantic, Geochemistry Geophysics Geosystems, 8, doi:10.1029/2006gc001360, 2007.

Xoplaki, E., Fleitmann, D., Luterbacher, J., Wagner, S., Haldon, J. F., Zorita, E., Telelis, I., Toreti, A., and Izdebski, A.:
630 The Medieval Climate Anomaly and Byzantium: A review of the evidence on climatic fluctuations, economic performance and societal change, Quaternary Science Reviews, 136, 229-252, doi:10.1016/j.quascirev.2015.10.004, 2016.
Wu, C.-J.: Max Planck Institute for Solar System Research, SATIRE-M reconstruction of spectral solar irradiance over the

Holocene, https://doi.org/10.17617/3.11, 2017.

Yamamoto, A., Abe-Ouchi, A., Ohgaito, R., Ito, A., and Oka, A.: Glacial CO2 decrease and deep-water deoxygenation by
635 iron fertilization from glaciogenic dust, Climate of the Past, 15, 981-996, doi:10.5194/cp-15-981-2019, 2019.

Zanchettin, D., Khodri, M., Timmreck, C., Toohey, M., Schmidt, A., Gerber, E. P., Hegerl, G., Robock, A., Pausata, F. S. R., Ball, W. T., Bauer, S. E., Bekki, S., Dhomse, S. S., LeGrande, A. N., Mann, G. W., Marshall, L., Mills, M., Marchand, M., Niemeier, U., Poulain, V., Rozanov, E., Rubino, A., Stenke, A., Tsigaridis, K., and Tummon, F.: The Model Intercomparison Project on the climatic response to Volcanic forcing (VolMIP): experimental design and forcing input
640 data for CMIP6, Geoscientific Model Development, 9, 2701-2719, doi:10.5194/gmd-9-2701-2016, 2016.

645

Table 1 Experimental settings for time-slice experiments

Experiment short name	PI	LGM	6ka	127ka
Time interval	Pre-industrial control (1850 CE)	Last Glacial Maximum (21,000 years before present)	6,000 years before present	127,000 years before present
Greenhous gas levels	CO_2 (ppm) 284.725 N_2O (ppb) 273.02 CH_4 (ppb) 808.25	190 200 375	264.4 262 597	275 255 685
Orbital parameters	Eccentricity 0.01672 Obliquity 23.45 Angular precession 102.04	0.018994 22.949 114.42	0.018682 24.105 0.87	0.039378 24.04 275.41
altitude	Present-day	ICE-6G_C	Same as PI	Same as PI
Dust	Calculated in the model	Calculated in the model with additional Erodibility map	Same as PI	Same as PI
Ice sheets and land-sea distribution	Present-day	ICE-6G_C	Same as PI	Same as PI
DOI	10.22033/ESGF/CMIP6.5710	10.22033/ESGF/CMIP6.5644	10.22033/ESGF/CMIP6.5646	10.22033/ESGF/CMIP6.5645

650

Table 2: Experimental settings for transient experiments with time varying forcing for LM

Orbital parameters	Berger 1978, Schmidt et al. 2011
GHG levels	Meinshousen et al. 2017
Solar irradiance	Wu et al. 2017
Volcanic forcing	Sigl 2015, Tooney and Sigl 2017
Land use	Laurence et al. 2016, Hurtt et al. 2017
Ozone	Scaled to solar UV irradiance
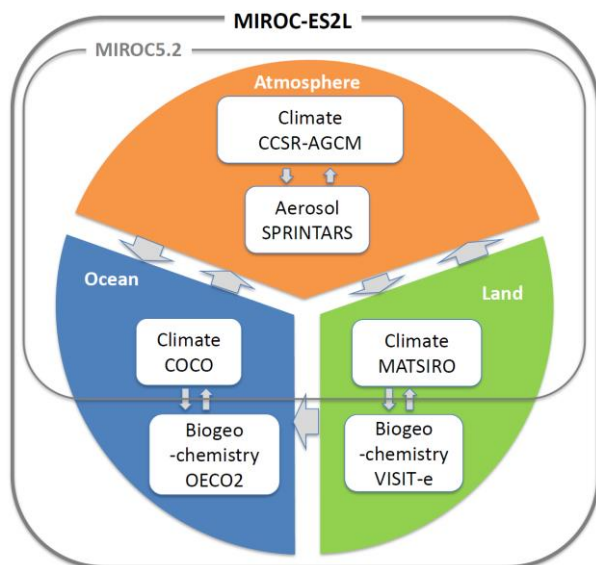
655   **Figure 1: Schematic of MIROC-ES2L.**

21
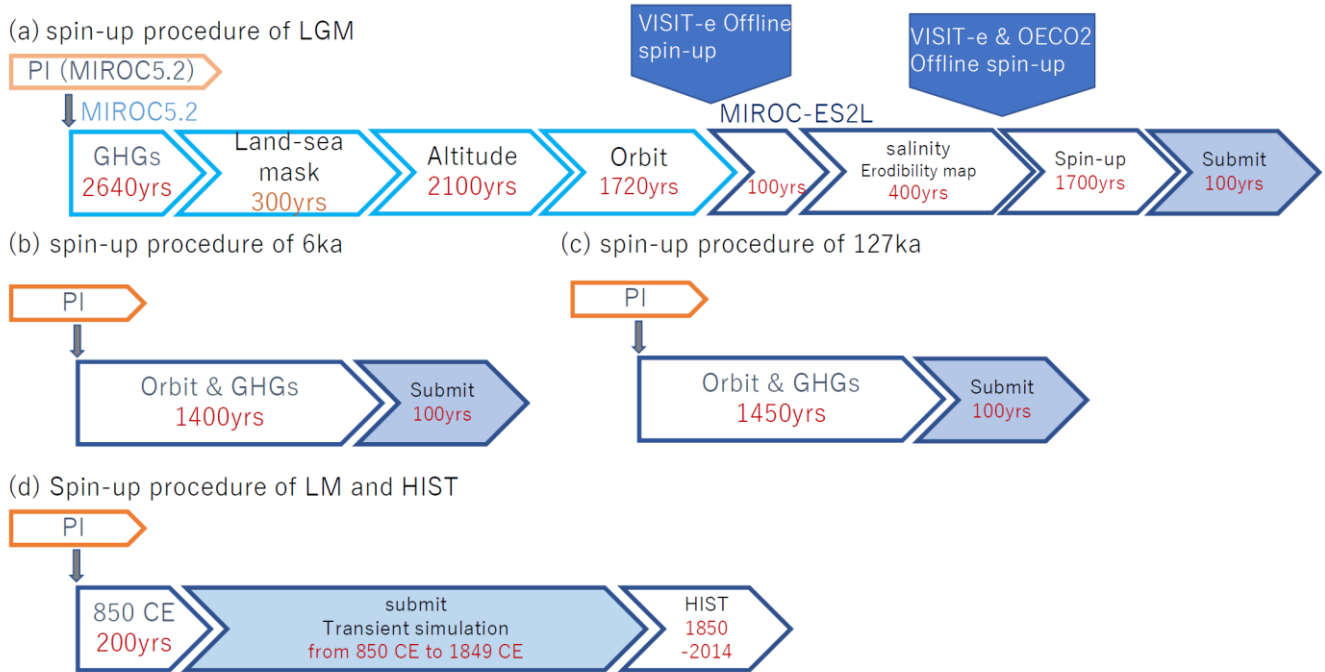
Figure 2: Schematic showing spin-up procedures of the following experiments: (a) LGM, (b) 6ka, (c) 127ka and (d) LM and HIST. Shapes with dark orange or blue outlines represent experiments using MIROC-ES2L. Shapes with light orange or blue outlines represent experiments using MIROC5.2. Shapes filled in pale blue represent model output submitted to PMIP4-CMIP6.
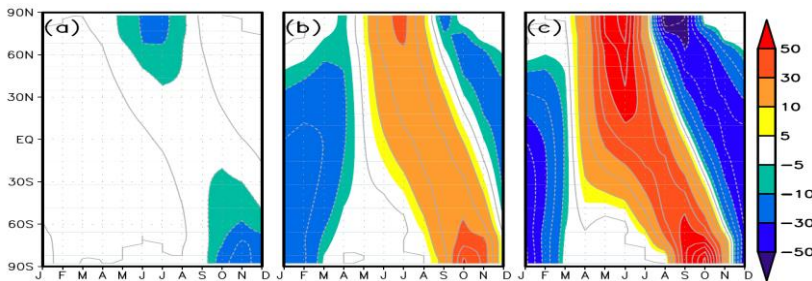
Figure 3: Variation of incoming shortwave solar radiation anomaly relative to PI (unit: W m^{-2}) with season and latitude for (a) LGM, (b) 6ka and (c) 127ka.
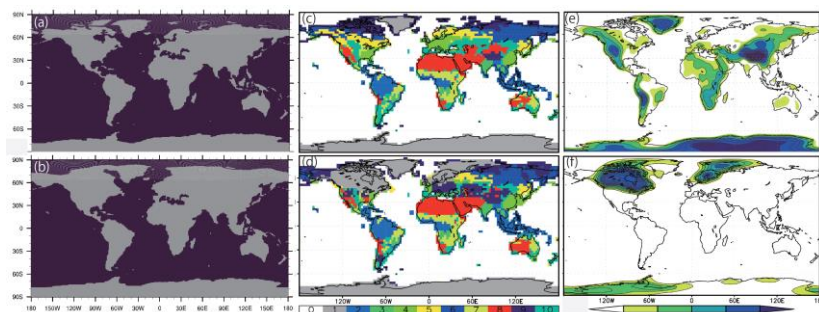
Figure 4: Left panels: Land–sea distribution converted to 1°× 1° ocean grids for (a) PI, 6ka, 127ka and (b) LGM. Middle panels: Distribution of land vegetation types for (c) PI, 6ka, 127ka and (d) LGM. Numbers in color bar represent vegetation types: 1) ice sheets, 2) broadleaf evergreen forest, 3) broadleaf deciduous forest and woodland, 4) mixed coniferous and broadleaf deciduous forest and woodland, 5) coniferous forest and woodland, 6) high-latitude deciduous forest and woodland, 7) wooded C4 grassland, 8) shrubs and bare ground, 9) tundra and 10) C3 grassland. Right panels: (e) Altitude for PI, 6ka, 127ka and LM (unit: m) and (f) altitude anomaly (unit: m) given for the LGM experiment based on ICE-6G_C (Peltier, 2015).
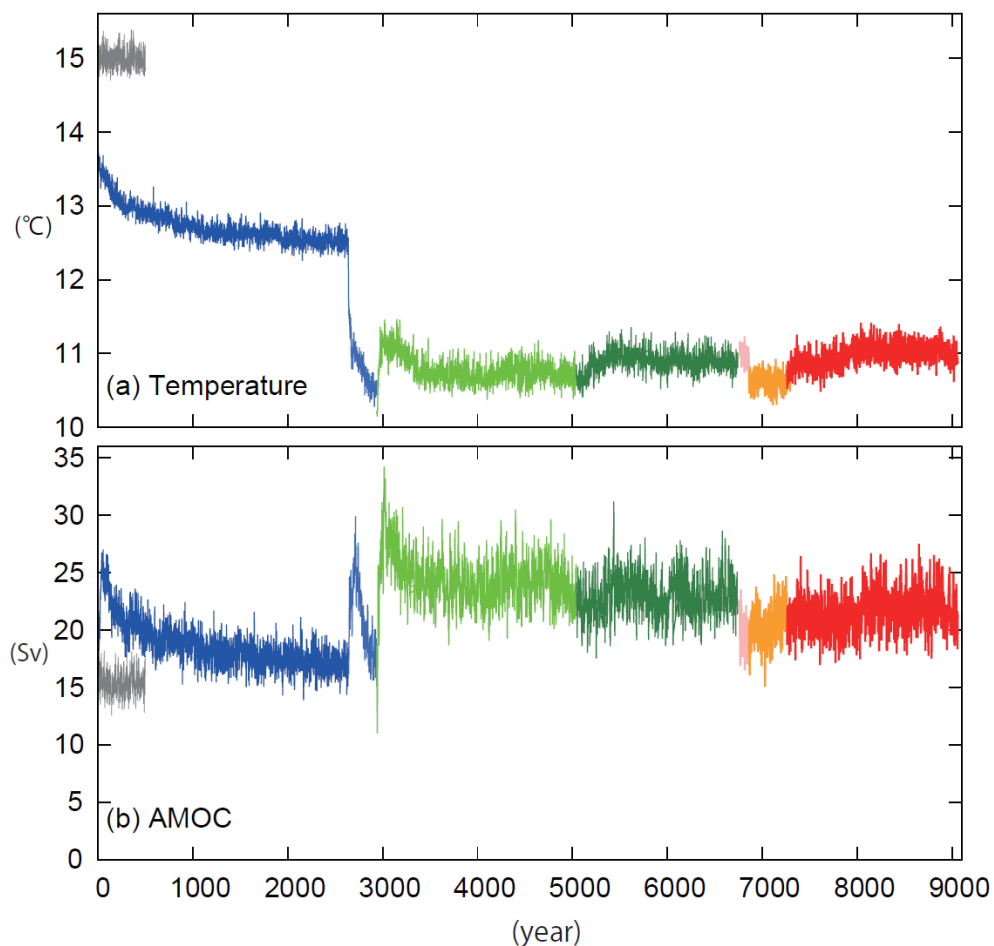
Figure 5: Time series for spin-up and submitted period (last 100 years) of LGM experiment and PI as a reference for (a) global mean air temperature at 2 m height and (b) peak values of annual mean AMOC. Gray line denotes PI value. Blue line: the experiment only GHG levels are set LGM. Light blue line: the land-sea distribution and land PFTs are changed to the LGM states. Yellow green line: altitude is set to the LGM state. Green line: orbit of the earth is set to the LGM values. Pink line: A spin-up experiment using MIROC-ES2L after VISIT-e offline spin-up. Orange line: The erodibility map and offset of ocean salinity are applied. Red line: The final spin-up after offline spin-up experiments by VISIT-e and OECO2.

680
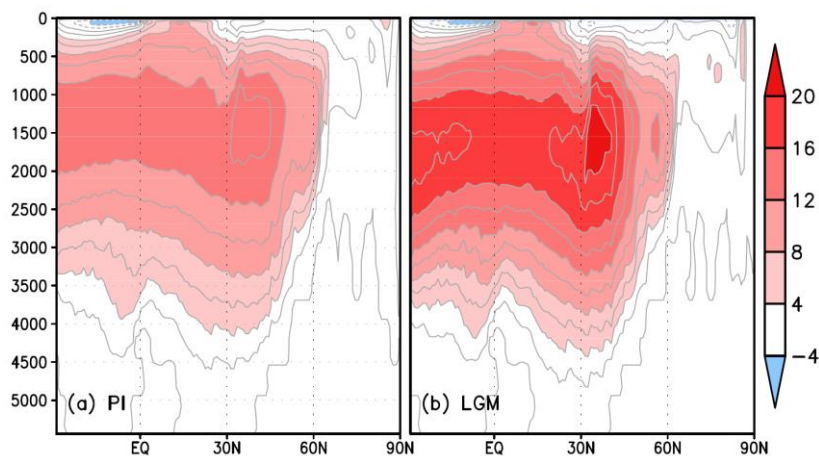
Figure 6: Meridional overturning streamfunction for the Atlantic basin (unit: Sv) for (a) PI and (b) LGM.
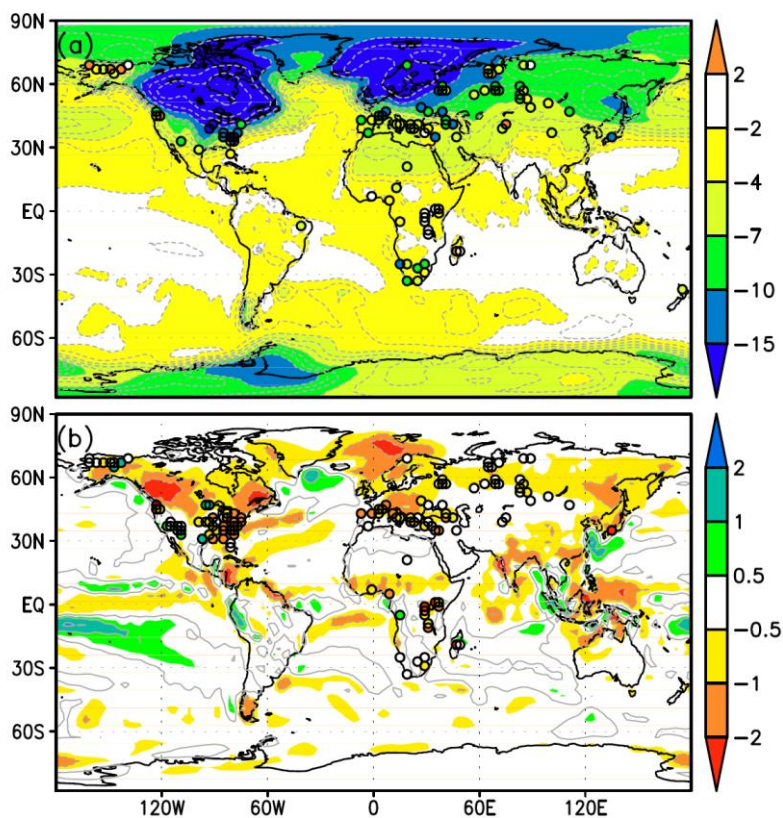
Figure 7: (a) Air temperature anomaly at 2 m height (unit: °C) and (b) precipitation anomaly (unit: mm day^{-1}). Anomalies are calculated as LGM relative to PI values. Circles denote values derived from proxy data (Bartlein et al., 2011).
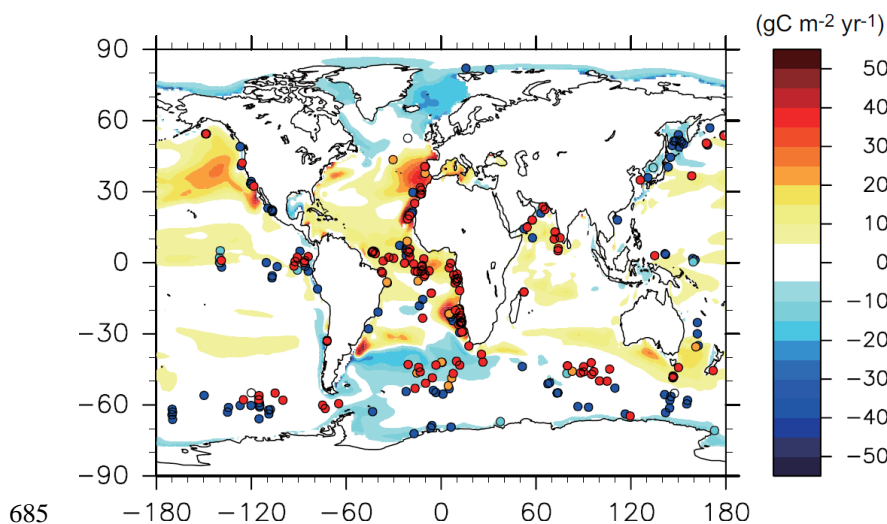
Figure 8: Primary production anomaly of the oceanic ecosystem (unit: gC m⁻² y⁻¹). Anomalies are calculated as LGM relative to PI values. Circles denote qualitative changes in primary production derived from proxy data (Kohfeld et al., 2013).
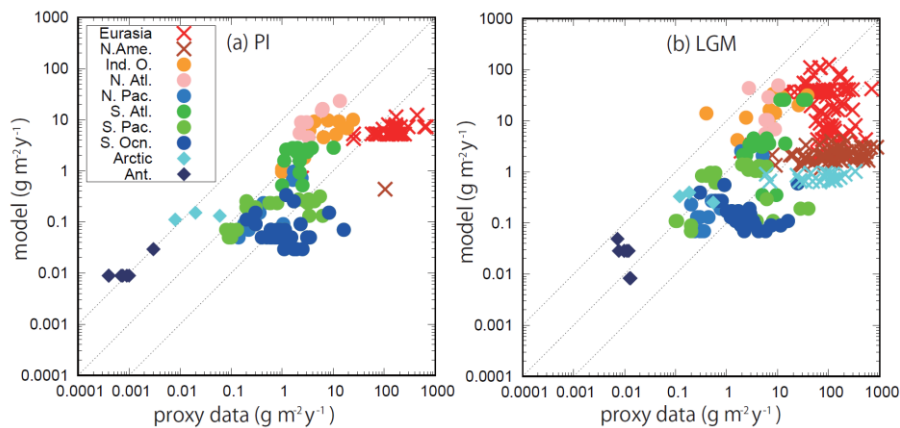
Figure 9: Dust deposition from model output and derived from proxy archives (Kohfeld et al., 2013; Albani et al. 2014) for (a) PI and (b) LGM (g m⁻² y⁻¹). Colors represent the locations of the proxy data, explained in the box in the figure. Crosses, circles and diamonds represent the terrestrial, marine, and ice core data.
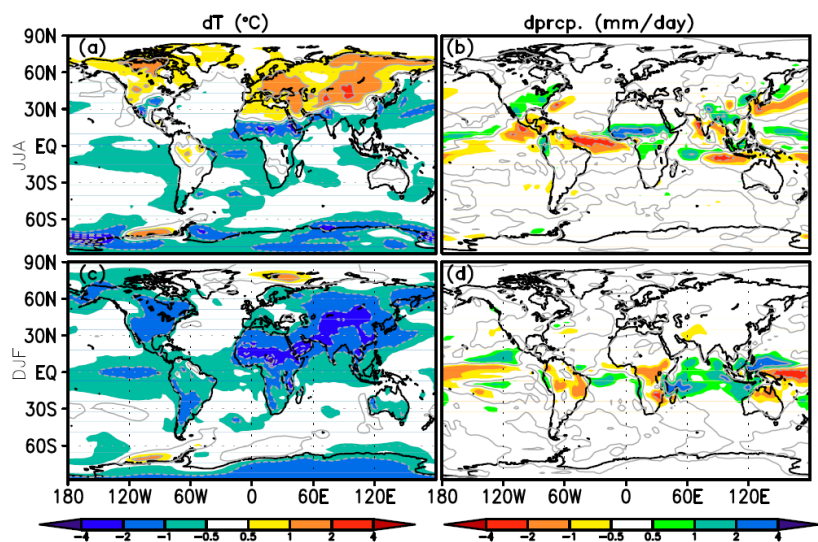
Figure 10: Seasonal temperature anomaly for (a) JJA and (c) DJF. Seasonal precipitation anomaly for (b) JJA and (d) DJF.
695 **Anomalies are calculated as 6ka relative to PI values.**
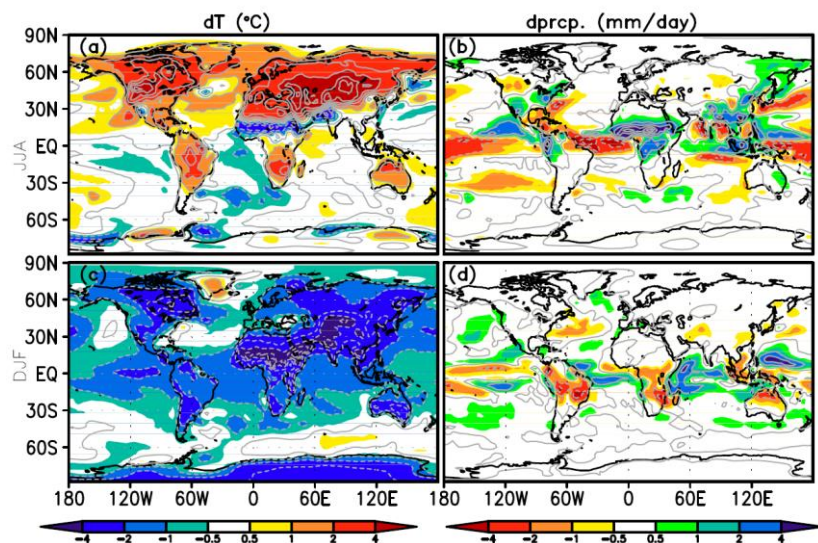

**Figure 11: Same as Fig. 10 but for 127ka.**

27
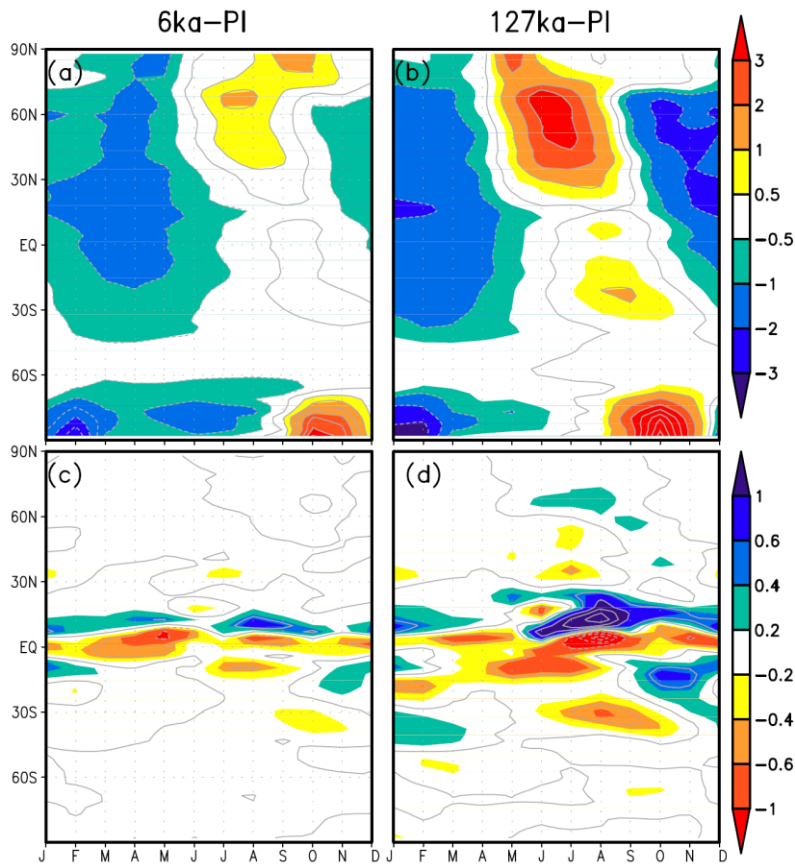
Figure 12: Hovmöller diagrams for (a) air temperature anomaly at 2 m height (°C) for 6ka relative to PI, (b) air temperature anomaly at 2 m height (°C) for 127ka relative to PI, (c) precipitation anomaly (mm day^{-1}) for 6ka relative to PI and (d) precipitation anomaly (mm day^{-1}) for 127ka relative to PI.
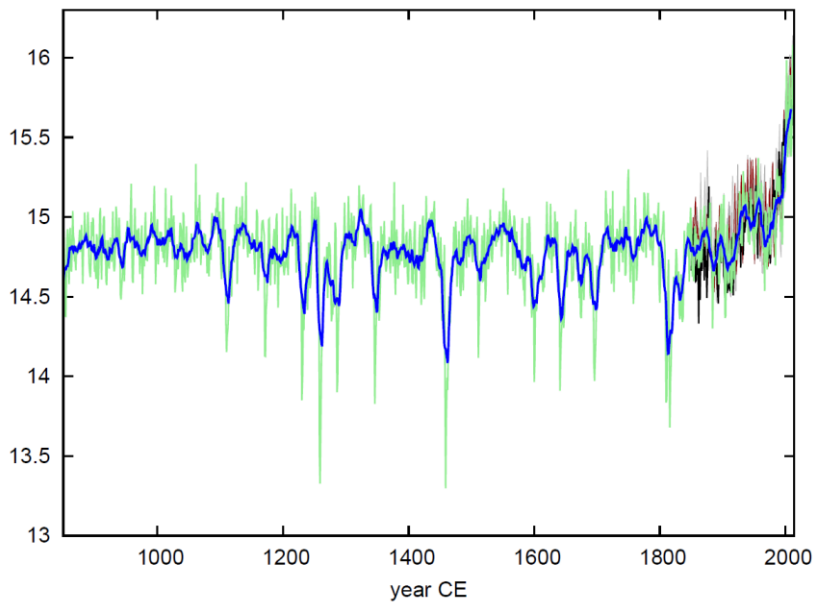
Figure 13: Annual mean air temperature (°C) averaged over the Northern Hemisphere from the LM and HIST experiments (green: annual mean, blue: 10 year running mean), from CMIP6 historical experiments (light gray: ensemble number 1, dark gray: ensemble number 2 and brown: ensemble number 3) and observational data from HadCRUT4 (black).

705